

Full identification of a growing and branching network's spatio-temporal structures.

Thibault Chassereau¹, Florence Chapeland-Leclerc¹, and Éric Herbert^{1,*}

¹Université Paris Cité, CNRS, UMR 8236-LIED, F-75013 Paris, France

*Corresponding author : eric.herbert@u-paris.fr

Compiled on July 10, 2024

Abstract

Experimentally monitoring the kinematics of branching network growth is a tricky task, given the complexity of the structures generated in three dimensions. One option is to drive the network in such a way as to obtain two-dimensional growth, enabling a collection of independent images to be obtained. The density of the network generates ambiguous structures, such as overlaps and meetings, which hinder the reconstruction of the chronology of connections. In this paper, we propose a general method for global network reconstruction. Each network connection is defined by a unique label, enabling it to be tracked in time and space. In this work, we distinguish between lateral and apical branches on the one hand, and extremities on the other. Finally, we reconstruct the network after identifying and eliminating overlaps. This method is then applied to the model filamentous fungus *Podospora anserina* to reconstruct its growing thallus. We derive criteria for differentiating between apical and lateral branches. We find that the outer ring is favorably composed of apical branches, while densification within the network comes from lateral branches. From this, we derive the specific dynamics of each of the two types. Finally, in the absence of any latency phase during growth initiation, we can reconstruct a time based on the equality of apical and lateral branching collections. This makes it possible to directly compare the growth dynamics of different thalli.

Significance

A complete description, i.e. both local and global, of a growing and branching network enables us to discuss the microscopic rules underlying emerging macroscopic phenomena. This task is made complex by the different scales involved, the high network density and network masking. Here, we propose a dynamics-based reconstruction method derived from a collection of bright-field images. We obtain a unique label for each structure, which can then be tracked in time and space, enabling their respective quantification during growth, and a first systematic classification of branches. These results pave the way for a better description of local rules and for realistic simulations.

Introduction

Networks are commonplace objects, and their study has been facilitated by the establishment of online databases Rossi and Ahmed [2015], Leskovec and Krevl [2014]. In this work, we are interested in growing spatial networks, which show a number of vertices and edges that increase over time, such as the layout of cities Lagesse et al. [2015], the propagation of cracks in drying clay Bohn et al. [2005], or the growth of a gorgonian Valcke [2020]. In nature, filamentous networks are ubiquitous (shoot and root systems of land plants, and in animal organs such as the lung, kidney, mammary gland, vasculature, etc) and constitute a key step in the evolution of morphological complexity Coudert et al. [2019]. What these networks have in common is a polarised growth process (at the end of the edges), a branching mechanism (new tip) and a merging mechanism (tip deletion). They generally are derived from time-lapse recordings and present the difficulty of reconstructing the dynamics from a collection of independent images. A representative example of such a growing branching network is the thallus of a mycelial fungus. Characterizing its growth is a tricky task. Hyphae form a complex, static yet growing network Falconer et al. [2005], without being able to define a homogeneous region of occupation, *ie* there is no clearly defined surface. In the literature, mycelia are usually described on a macroscopic scale using quantities such as mass or apparent thallus diameter. However, the filamentous nature of the mycelium makes these quantities unsuitable. It is therefore no longer possible to distinguish the different phenomena at work during growth, which would enable us to characterize different species, stresses or mutants Ledoux et al. [2024]. For example, connection rates, or the difference in density between the centre and the periphery. The initiation phase was also rendered inaccessible as the thallus had barely formed and was too small for macroscopic measurement Ulzurrun et al. [2019], De Ligne et al. [2019].

At the microscopic level, studies were limited to localised manual surveys on analogue and then digital images until the 2010s, using white light Boswell et al. [2002], Bebbler et al. [2007], Trinci [1973a,b], Fricker et al. [2008], Reynaga-Peña et al. [1997] or, more rarely, radionuclides Gooday [1971]. Automation of the image acquisition and processing has enabled a new experimental period to be opened up. Specific observables (such as length, orientation etc) can be quantified over time, by monitoring single hypha but the global dynamics become then inaccessible Barry et al. [2009], Sánchez-Orellana et al. [2018], Schmieder et al. [2019]. The entire mycelium has also been studied in two dimensions Vidal-Diez de Ulzurrun et al. [2015], Fricker et al. [2017], Dikec et al. [2020] and three dimensions using confocal laser scanning microscopy Du et al. [2016] (see also Chiang et al. [2011] that consider Brain-wide Wiring Networks in *Drosophila*) or X-ray microcomputed tomography Schmieder et al. [2019]. These observations were used to discuss changes in overall length, exhaustive collections of free apexes, fraction of biomass and branch angles using specific software, generally based on graphical reconstructions of the network. These approaches consider collections of independent images, so it is not possible to automatically track an apex through time. Overlaps, and in particular the distinction with network connections, are then particularly tricky to deal with, even when relying on a 3-D reconstruction Chiang et al. [2011].

Basing our analysis on the kinematics of the network’s growth, we propose in this paper a complete reconstruction method that associates a unique identifier with each node in the network across time and space. It then becomes possible to automatically track the exhaustive collection of network apexes over time. We will focus our analysis on *Podospora anserina* Silar [2020], a coprophilous filamentous ascomycete, a large group of saprotrophic fungi, that mostly grows on herbivorous animal dungs and plays an essential role within this complex biotope in decomposing and recycling nutrients from animal feces. Then, *P. anserina* can be considered as a short-range

forager, displaying usually highly dense hyphae that are successful in encountering small organic food resources (Sanati Nezhad and Geitmann [2013]). *P. anserina* has long been used as an efficient laboratory model to study various biological phenomena, especially because it rapidly grows on standard culture medium, it accomplishes its complete life cycle in only one week, leading to the production of ascospores, and it is easily usable in molecular genetics, cellular biology and cytology. *P. anserina* is a model for studying the growth of biological networks, as the its thallus shows great complexity, but its growth follows a simple set of rules. We recall some details concerning the thallus growth of *P. anserina*: (i) growth is highly polarized, *ie* it occurs only through the apex of the hyphae, (ii) once formed, the hyphae are immobile, (iii) a new hyphae is created during the branching process, which generates a new apex. It can be located near an existing apex or elsewhere on the network (iv) when two hyphae meet they may fuse (anastomosis).

In this work, we build on a graph structure to describe this network, since these rules can be easily translated. First, the initial spore is the only permitted origin of the network. The network is static ; *ie* hyphae grow in length but do not move or disappear. The network is considered to grow only in 2D ; the only vertical movement permitted is overlap. Hyphae are always in contact with the substrate. The temporal dynamics of growth allow causality (the network must be contiguous).

We extract the information needed for a complete description, in space and time, of the network growth. We identify and label each biologically relevant vertex (also called node) to enable individual temporal tracking of each vertex, disambiguating the different types of crossover based on the spatio-temporal dynamics of the growing network. Building on the vertex collections we’ve built, we then quantify each type of branching over time. Our method allows to (i)–label each network vertex with a unique identifier, enabling it to be tracked over time. In particular, we plan to indicate the location and time at which each vertex appeared. (ii)–At each time step, the growth of each hypha, *ie* the displacement of each apex, is measured. Each apex is identified in time and space and connected to the correct branch. Lateral branches are distinguishable from apical branches. The direction of growth is regained. (iii)–Distinguish between branchings (connections), anastomoses (fusions) and overlaps for each degree-3 vertex. Overlap are eliminated from the network connections list and the corresponding network reconstructed accordingly. Finally, complete hyphae, from the branching to the apex, are reconstructed.

Materials and methods

In this section we will briefly discuss the *experimental setup*, largely described elsewhere. Then we describe the reconstruction process of the network spatio-temporal structure. In the subsection *Temporal coordinate* we will see how a temporal coordinate is set to each node in the network. The subsection *Branch identification and twig’s orientation* will focus on how we define and identify each branch in the network. The last subsection *Degree-3 vertices classification and overlaps* will deal with the classification of each degree-3 vertices according to its biological nature and the detection of overlaps.

Experimental setup

In, Dikec et al. [2020], Ledoux et al. [2022, 2023] we discussed the global growth of hyphal network expansion and structure of *P. anserina* under controlled conditions based on the temporal series of centimetric image size, with a typical micrometric resolution, of the network dynamics, starting from germinating ascospores. An experimental device allowing to solve the dynamics of the local

and global growth of the complete hyphal network of *P. anserina* directly on a Petri dish from an ascospore and over a period of approximately 20 hours in a controlled environment has been previously developed and described in Dikec et al. [2020]. We did use of this setup to carry out three, named (A), (B) and (C) thereafter, complete and independent series of a collection of greyscale images of the thallus growth, from a single initial micrometric spore to a complex network of thousands of interconnected hyphae, under standard growth conditions with M2 culture medium, see Silar [2020] for more details, at an optimal temperature of 27°C. A sheet of cellophane is placed on top of the culture medium. The porosity of this sheet allows the nutrients to pass through and nourish the growth of the thallus and its rigidity prevents the apexes from penetrating into the nutrient medium and keeps the network at its surface. The growth of the network is then driven mostly in two dimensions during the observation period. It leads to a series of grey-scale images taken every $T = 18\text{min}$ with a spatial resolution of $1.6\mu\text{m}/\text{pixel}$. No confinement is imposed at the top of the network, allowing hyphae to cross each other by overlapping. As the camera is fixed above the thallus, the images obtained are the projection of the entire network on this axis. Thus, the connections observed on the network images may be real, *ie* composed of branches or anastomoses (fusion of hyphae) or artifacts, *ie* overlaps. The distinction between branches, anastomoses and overlaps is then made impossible, preventing the simple numeration of significant biological objects, the branches, apart from an approximate accounting, as proposed in Dikec et al. [2020]. A crucial part of the work presented in this article is to propose a method of disambiguation of the different connection types. The standard binarisation and vectorization process described in Dikec et al. [2020] allowed for extracting the associated digital network independently for each image. The objects making up the network are not identified identically in each image, which means they cannot be tracked individually over time. These digital networks correspond to graphs made up of degree 1 vertices (corresponding to the apexes), degree 2 vertices (corresponding to the hyphal skeleton) and degree 3 vertices (corresponding to branches, mergers, encounters and overlaps). Vertices with more than 3 connections are rejected as having no biological significance. Typically, overlaps appear as two vertices of degree 3.

Temporal coordinate

Direct vertex dating. As the hyphae of *P. anserina* can only grow and not move, every point in the network present at a time t_1 is present for all $t_2 \geq t_1$. Consequently we derived only one graph of the network from the last image of our experiment. Each hypha is then allowed to grow only in this network. Vertex location is determined by the final network graph. Growth is understood as the time at which each node appears. Therefore the goal here is to find, for each node of the network, at which time t_0 the node is present for the first time. As in our setup, hyphae appear white on a black background, t_0 is calculated from the evolution over the time t of the luminosity intensity I of the pixels around the node. Theoretically, we expect to see a step function with the following expression:

$$S_{t_0}(t) = \begin{cases} I_{background} & \text{if } t < t_0 \\ I_{hyphae} & \text{if } t \geq t_0 \end{cases} \quad (1)$$

For each pixel that is activated in the final binarized image, we find the best fit for the parameter t_0 through least square method, see figure 1. $I_{background}$ and I_{hyphae} are chosen to be the mean gray level value respectively before and after t_0 . For each pixel around the node, we find the value for t_0 that minimize the deviation from the step function. The first estimation of t_0 for the node is then the minimal value for this parameter among those pixels. This selection is set to take all

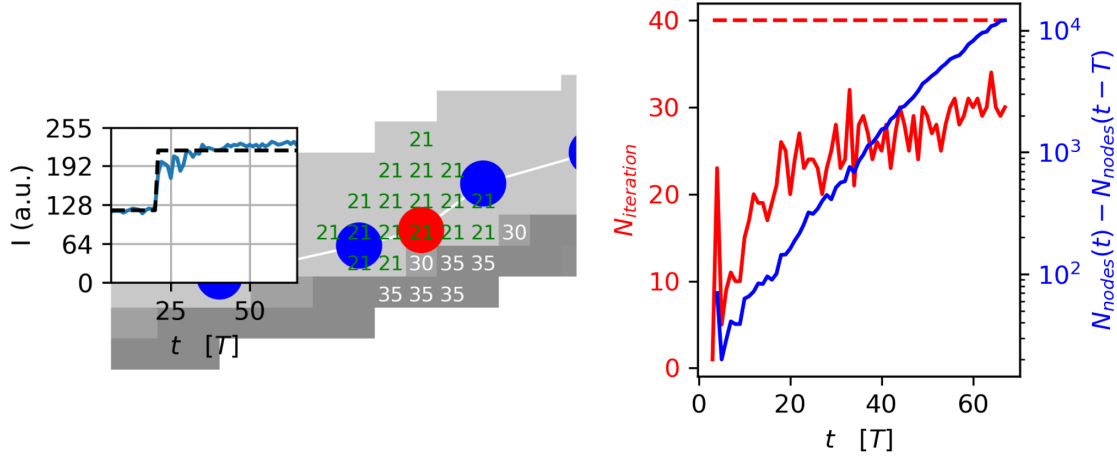


Figure 1: Left) Example of time coordinate estimation of a node of interest here in red. Each pixel in the area of interest is marked with the t_0 value estimated by fitting the step function (see Equation 1) colored in green if it correspond to the minimum value in the area of interest. The insert is an example of the variation in pixel's gray level over time (in blue) and black dashed line correspond to best fit. Right) Number of iteration needed $N_{iteration}$ and number of added nodes for each frame. Red dashed line corresponds to the threshold value over which a potential issue is detected.

pixels within half a hyphal diameter of the node (a hypha is estimated to be 7 pixels wide). This method requires good contrast of luminosity between the hyphae and the background.

The vast majority of nodes can be dated in this way. Locally, however, binarization may have been biased by the presence of impurities or a loss of focus. This leads to two problems, which we address in turn below. The correction of a poor estimate of t_0 and the correction of a hyphae discontinuity. **Correction of wrong estimation of t_0 .** As all nodes are connected, an erroneous estimate of t_0 can simply be identified by comparing it with the t_0 of its nearest neighbors. Each node must be framed by an older and a newer node. Once a spurious estimate is detected for a specific node, the corresponding t_0 is replaced by an arithmetic mean of the nodes surrounding it. For each new frame, only the vertices with a first estimate of t_0 lesser or equal to the current frame and neighbor of an already added vertex are added to the growing network. For a given frame, we repeat this step as long as we add at least one new point and we keep track of the number of iteration needed. To initialize this process we use the first image binarized as a mask to identify the starting nodes of the network. **Correction of broken edges** In the case of impurity or loss of focus, the density contrast may be insufficient for binarization to detect the hypha. These defects appear as discontinuities. In our procedure, nodes are added with a continuity condition. Breaking an edge stops the procedure, and prevents further identification of the growth. The network features a large number of branches and crossings. So it's extremely likely that the hypha is connected via another part of the network. It will eventually be added to the network, but in a particular way, *ie* the entire length will appear in a single time step. These situations are detected and manually corrected (generally by reconstructing the continuity of the incident hypha). The network is reconstructed

from contiguous vertices. Branches thus appear spontaneously as dated vertices in a previously existing segment. The dating of branches is reconstructed as the instant when the length of the considered hypha is zero. We now have the network of dated vertices. We now turn our attention to branch reconstruction.

Branch reconstruction and orientation

The vertices form interconnected filaments, or hyphae, which are the structure of the network. We are now going to reconstruct each of these hyphae using the time-space coordinates of the collection of vertices defined in the previous section. The definition of a hypha as a long filament which collectively form the mycelium is a little vague. To avoid any confusion and in order to generalise the problem to non-fungal networks, we introduce the notion of branch, defined as the set of vertices in the network corresponding to the trajectory of an apex. In the remainder of this document, we will use the terms *hyphae* and *branches* interchangeably. At first glance, a branch is easily identified as a succession of degree-2 nodes between a degree-3 node corresponding to the initial branching of the branch and an apex represented by a degree-1 node. A branch may also terminate with a degree-3 node when it merges with another hypha. However, this branch will itself be the origin of other branches and may be the site of anastomosis of other branches. The collection of vertices that make up the branch is therefore more varied and complex. We can think of it as a series of degree-2 vertices, each framed by vertices of degree-3 and/or 1. We define these series of degree-2 nodes between two degree-3 or degree-1 nodes as twigs (called terminal twigs if they end in a degree-1 node). A branch is then a succession of twigs. Let us now turn to the collection of twigs to be chosen to reconstruct a branch. Assuming that all the twigs are oriented in the direction of growth of the network, identifying the branches means associating locally, at each degree-3 vertex, which twigs correspond to the same branch. Each degree-3 vertex must follow one and only one of the following four rules:

- Source: three outgoing twigs. From a biological point of view, as we start from a unique spore, this source can only be unique too. Each outgoing twig is considered to be the starting point of a new branch.
- Wells: three incoming twigs. This case corresponds to 3 apexes in the same place at the same time. Although rare, this configuration is permitted during reconstruction. The three corresponding twigs are considered to be the terminations of their respective branches.
- Branching: two outgoing twigs and one incoming twig.
- Meeting: one outgoing twig and two incoming twigs.

Those different cases are shown in the figure 2.

Based on the previous rules, we deduced the direction of growth of each twig incrementally. The boundary conditions are the collection of the direction of the terminal twigs, that can be determined without any ambiguity. We then propagate the rule for orienting the terminal twigs recursively. The initial spore is the only one source allowed. If our network contains no encounters, all directions of all branches are found in this way.

However, since it is not the case, some twigs orientation remain undecidable with this single step especially in the denser center of the network. To achieve this, we have built a second step based on a confidence level c_k for each twig k that depends only on the direction of the apex during the twig

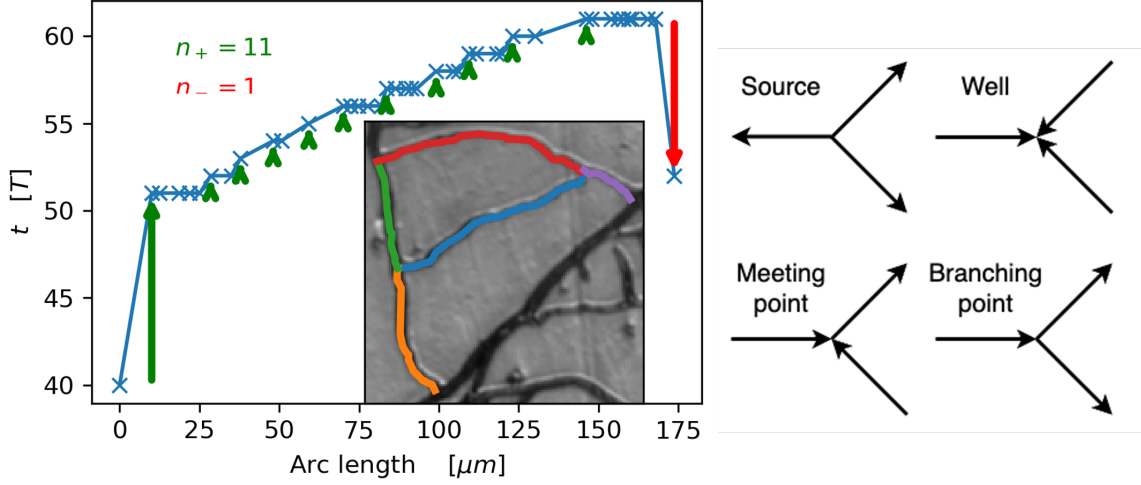


Figure 2: Example of apparition time vs the arc length for nodes along a twig. Increment and decrement are indicated by respectively green or red arrows. Inset shows the corresponding picture of the network with in blue the twig of interest and its neighbor twigs.

formation. For a given orientation we note n_+ the number of temporal increments (positive change in the time coordinate when traveling along the twig) and n_- the number of temporal decrements (negative change in the time coordinate when traveling along the twig). The confidence level is then defined by the following equation:

$$\forall k \in \{\text{twigs}\}, c_k = \frac{n_+ - n_-}{n_+ + n_-} \tanh\left(\frac{n_+ + n_-}{\mathcal{N}}\right) \quad (2)$$

Where $\mathcal{N} > 0$ is a constant used to set the number of increments by which the user can really be confident about the direction of the twig. We made use of $\mathcal{N} = 3$. With this expression, c_k varies between $+1$ if the initial direction (define as the one verifying $n_+ \geq n_-$) of the twig is in agreement with the growth directions of each time step and -1 in the opposite way. Changing the direction of growth of the twig simply corresponds to switch n_+ and n_- and change the sign of c_k . This confidence alone is sufficient to find the correct direction for twigs long enough to contain several increments, but for shorter twigs it is not adequate. To this end, we introduce a score s_k combining this confidence level and the alignment with the neighbouring twigs $\mathcal{V}(k)$ following the equation:

$$\forall k \in \{\text{twigs}\}, s_k = c_k + \alpha(1 - |c_k|) \sum_{\ell \in \mathcal{V}(k)} \mathbf{u}_k \cdot \mathbf{u}_\ell c_\ell \quad (3)$$

With $\mathbf{u}_{k,\ell}$ the unit direction vector of the twig and α a coefficient used to gauge the relative importance of alignment in relation to confidence. Typically we set $\alpha = 1/4$ as there is 4 neighbouring twigs. This allows to give the same weight for space and time. We then assume the best orientation of the remaining twigs is given by the maximisation of the total score of the network, defined as the sum of all local score. We achieve this by using a Monte-Carlo algorithm where we check in a random order all twigs and switch there orientation with a certain probability defined by the

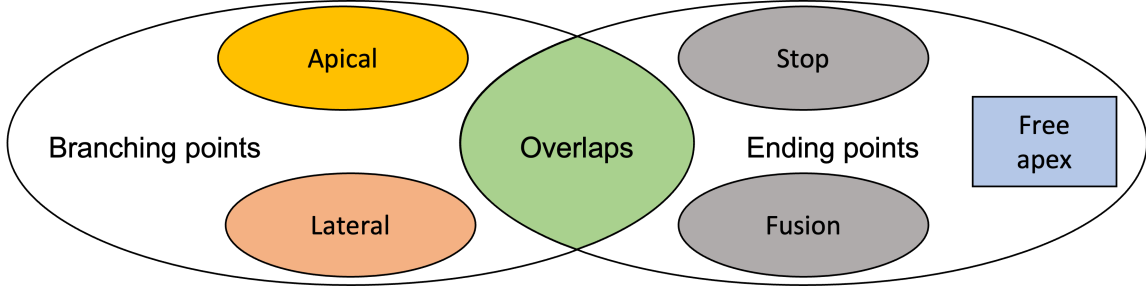


Figure 3: Distinction between the degree of network vertices and their associated biological natures. A degree-3 vertex may be due to a branching point which itself may be of two types (apical or lateral) but may also be the result of the meeting of two hyphae. In the case of a meeting, it is not possible to differentiate between anastomosis (fusion) and simple growth stop.

score’s variation induced. The Monte-Carlo “temperature” β is set to 1 and then doubled every hundred iterations. The process is stopped when the acceptance rate is below 1% or after reaching $\beta = 1024$.

Degree-3 vertex classification and overlaps

As already discussed in the previous section, due to the image acquisition procedure, degree-3 vertices correspond to a collection of objects of different natures. Some are biologically relevant, others are not. First correspond to branching points, *ie* the departure of new hyphae, while others correspond to the meeting of two hyphae. Meeting point can be divided into two sub-categories. Anastomosis, *ie* fusion of two hyphae, and encounters, if an apex arrives and stops growing close to a previously existing hypha. In the same way branching points can be divided into two sub-categories. Apical and lateral branching points, depending on the distance between the branch and the apex at the time of branching. Overlaps are a population to be identified in order to correct spurious connections. Indeed, each overlap add two false degree-3 vertices, one appearing as a new branching point and the other one appearing as an encounters. This whole zoology of events is summarised in the figure 3. Let-us now turn to the detection and classification of overlaps. The difficulty here comes from the particular topology of the crossing, that, in most cases, can not be reduced to simple crossing of two straight lines. As an example, the overlapping hypha may follow the overlapped hypha before resuming its own trajectory which, with a naive approach, would lead to the detection of two false branches. Conversely, an apex intercepting an hypha close to a previously existing branch would lead to the detection of a false overlap.

We first consider all triplets of branches $(B_{carrier}, B_{in}, B_{out})$ where $B_{carrier}$ is the branch corresponding to the overlapped hypha, $B_{in/out}$ correspond to the incoming/outgoing part of the overlapping hypha. For the triplet to be a valid overlap, we checked a spatial and temporal conditions. (i)-Connection condition: B_{in} must end with a degree-3 vertex connected to $B_{carrier}$ and B_{out} must start with a degree-3 vertex connected to $B_{carrier}$. We then derive the arc length L_o corresponding to the distance between these two vertices. We set a threshold on L_o , typically a few hyphae diameters at which we consider that the triplet is no longer a potential overlap.

(ii)-Temporal condition: B_{out} branch must have started its growth after the B_{in} branch have arrived at the crossing. In fact, if we note Δt_o the difference between the time of B_{out} ’s growth start

and the time of arrival of B_{in} , we must have $V\Delta t_o \approx L$ with V the typical elongation rate of the network.

Finally, of all the remaining triplets satisfying the above conditions, each branch can appear at most once as an incoming branch and at most once as an outgoing branch. If a branch appears several times in one of these roles, we keep only the triplet corresponding to the best alignment between the B_{in} and B_{out} branches. When the overlap is confirmed, we disconnect the incoming and outgoing branches from the carrying branch and reconnect them together via a new node labeled negatively (to keep track of the overlap) situated at the mean position of the overlap. Therefore, the two degree-3 vertices become two degree-2 vertices along the carrying branch and the incoming and outgoing branches become the same branch.

Results

Overlap detection performance

In order to estimate the performance of the overlap detection we build a simulation reproducing the different configurations observed. Branching process are allowed to occur on two parallel branches of constant length. Contact with the second hypha will randomly cause overlaps or encounters as shown in figure 4. The two parameters of this simulation are $h = \frac{H}{V T}$, the distance between the two main branches normalized by the growth rate, and $\ell = \frac{L}{V T}$ the distance between two events along the main branch normalized in the same way. We set $N_{test} = 100$ the number of events occurring along the main hyphae ; each (h, ℓ) configuration is reproduced ten times. To quantify the performance of the detection, we made use of usual binary classifications Chicco and Jurman [2020]. Precision $P = \frac{TP}{TP+FP}$, recall $R = \frac{TP}{TP+FN}$, F-score $F = 2 \frac{PR}{P+R}$ and the normalised Matthews correlation coefficient $nMCC = (MCC + 1)/2$ (with $MCC = \frac{TP TN - FP FN}{\sqrt{(TP+FP)(TP+FN)(TN+FP)(TN+FN)}}$) are calculated and reported in the figure 4 for various values of (h, ℓ) around the typical range of values encountered in the experiments, with TP the number of true positive overlap detection, FP the number of false positive, FN the number of false negative and TN the number of true negative. The main result of P and R shown in figure 4 is that, except in a region where hyphae cannot be distinctly separated (both ℓ and h are small), detection quality is very good and relatively independent of ℓ and h . More precisely, R is found to be maximal, *ie* FNs are very infrequently observed. P is found in the range 0.7-0.9, which means a detection bias in favor of FP. Some branching are counted as overlaps. By combining the quantities R and P , F-score summarizes the quality of the classification method used. F-score ignores the count of True Negatives (TN). Because TN are supposed to be numerous, it is interesting to take into account all elements of the confusion matrix. We find that $nMCC \sim 0.85$, a high confidence value, throughout the region of interest.

Distinction apical/lateral branching

Reduced to the most succinct list, the rules for network growth appear to be few. The first is polarized growth, the second is connection capacity. As shown in figure 3 degree-3 vertices can be divided into two sub-populations, namely the lateral and apical branching points. It seems odd that different processes are used to generate the same property. However in the literature the distinction between the two types is routinely made using the location of their connection to the hypha. At the apex in the apical case, further away in the lateral case. This phenomenological distinction is

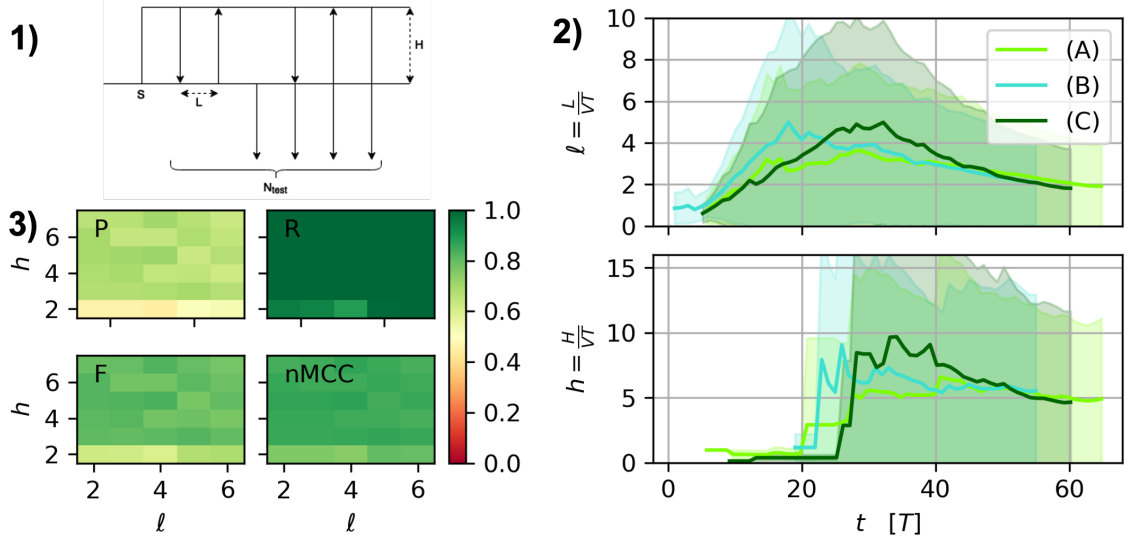


Figure 4: 1) Schematic diagram of the simulation reproducing the different hyphal encounter configurations. For each pair of H and L parameter values, ten simulations each generate $N_{test} = 100$ events randomly selected from the different encounter cases. 2) Measurements in the 3 networks (A), (B) and (C) of the $l = L/VT$ and $h = H/VT$ values encountered over time (mean + std). 3) Average precision P , recall R , F-score F and normalized Matthew Correlation Coefficient $nMCC$ of simulations as a function of l and h values.

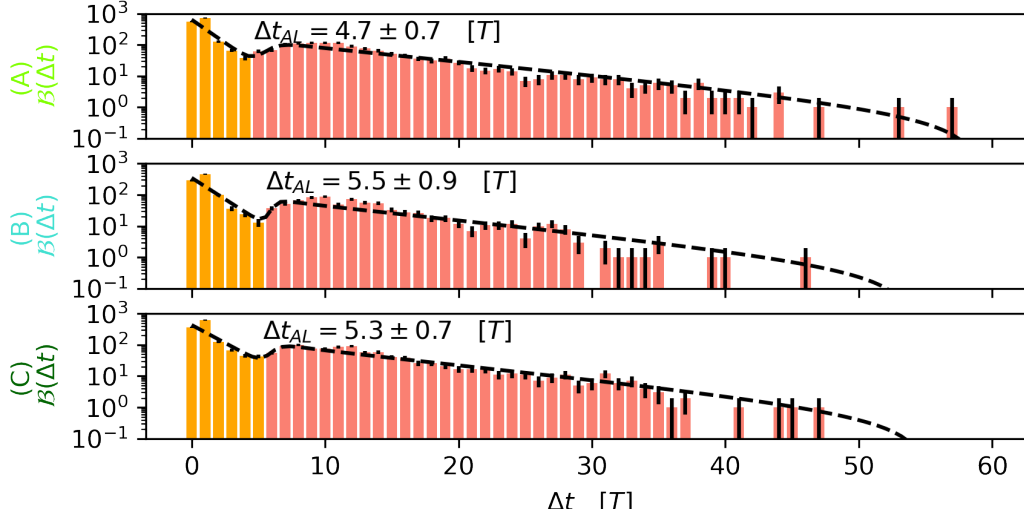


Figure 5: Distribution of latency times before branching for the three experiments. The black dashed line corresponds to the best fit based on equation 4. Numerical values of the parameters of dashed lines are in table 1. The vertical solid black line corresponds to the value of Δt_{AL} calculated according to equation 5 and used to distinguish between apical branches (in orange) and lateral branches (in red).

linked to a lower growth rate for hyphae coming from lateral branching. In Ledoux et al. [2023] we proposed a classification criterion based on the distance apex/branching point, but it was not systematically evaluated on the whole thallus, making it possible for a bias to exist. In this section, building our analysis on the complete thallus we propose a definitive criterion to clearly distinguish between apical and lateral branching. To remove the ambiguity of the distance to the apex during encounters, we look instead at the latency time Δt between the first passage of the mother branch and the time the new branch starts to grow as shown in figure 5.

We observe a bi-modal distribution where we assume that the first mode corresponds to the apical branching process while the second is the result of lateral branching process. In fact, by looking at a single branch at a given time we can easily convert the latency before branching to a length from the tip assuming a constant elongation rate. Therefore the shortest latency are closest to the tip and should correspond to apical (or sub-apical) branching points. We can express $\mathcal{B}_{t_i}^{t_f}(\Delta t)$ the number of branching observe between the instant t_i and t_f corresponding at a latency of Δt as the sum of the corresponding apical branching points $\mathcal{A}_{t_i}^{t_f}(\Delta t)$ and lateral branching points $\mathcal{L}_{t_i}^{t_f}(\Delta t)$. Assuming that apical branches are distributed according to an exponential law (parameter ω_A) with respect to the apex and that lateral branches are uniformly distributed along the hypha except for an exclusion zone near the apex (modelled by a sigmoid centred at m and with slope s) one can

Experiment	(A)	(B)	(C)	Mean
N_0	3.19 ± 0.09	3.7 ± 0.2	1.9 ± 0.1	Not applicable
$\nu[h^{-1}]$	0.506 ± 0.003	0.540 ± 0.004	0.570 ± 0.006	0.539 ± 0.006
$L_0[mm]$	1.09 ± 0.05	1.52 ± 0.08	1.00 ± 0.04	Not applicable
$\lambda[h^{-1}]$	0.476 ± 0.004	0.501 ± 0.005	0.508 ± 0.004	0.495 ± 0.003
$\tau_A[h^{-1}]$	0.15 ± 0.02	0.16 ± 0.02	0.18 ± 0.02	0.16 ± 0.01
$\omega_A[h^{-1}]$	2.3 ± 0.2	2.1 ± 0.3	1.8 ± 0.2	2.0 ± 0.2
$\tau_L[h^{-1}.mm^{-1}]$	1.1 ± 0.1	0.9 ± 0.1	1.2 ± 0.1	1.06 ± 0.06
$m[min]$	105 ± 7	110 ± 6	111 ± 6	109 ± 4
$s[min]$	10 ± 6	5 ± 8	7 ± 6	8 ± 4
$\Delta t_{AL}[min]$	84 ± 13	100 ± 16	96 ± 13	93 ± 8

Table 1: Numerical values from the fit of latency from figure 5 according to equation 4. Δt_{AL} is calculated from m and s as in 5.

show that $\mathcal{B}_{t_i}^{t_f}(\Delta t)$ is given by (see appendix for more details):

$$\begin{aligned} \mathcal{B}_{t_i}^{t_f}(\Delta t) = & \tau_A \frac{N(t_f) - N(t_i)}{\nu \log 2} e^{-\omega_A \Delta t} \frac{1 - e^{-\omega_A T}}{1 - e^{-\omega_A(t_f - t_i + T)}} \\ & + \frac{\tau_L}{1 + e^{-(\Delta t - m)/s}} (1 - 2^{-\lambda T}) \frac{L(t_f - \Delta t) - L(t_i)}{\lambda \log 2} \end{aligned} \quad (4)$$

With $(L_0, \lambda), (N_0, \nu)$ the parameters of the exponential fit of respectively the total length of the network L and the total number N of branching points. We can then define Δt_{AL} , the threshold below which the branch is considered apical as the "starting point" of the lateral branching sigmoid:

$$\Delta t_{AL} = m - 2s \quad (5)$$

We find that $\Delta t_{AL} = 93 \pm 8[min]$.

Distinctions between apical and lateral branches

Temporal distinction: This distinction allows us to monitor the respective number of apical and lateral branches over time as we can see in figure 6. Both follow an exponential growth of the form:

$$N_X = N_X^0 2^{\nu_X t} \quad (6)$$

At first, branches come only from apical branching. However, the effective rate of lateral branching is greater than that of apical branching. This leads to the point where both kind of branches are present in equal number. We can extract this time t_{eq} when $N_A(t_{eq}) = N_L(t_{eq}) = N_{eq}$:

$$t_{eq} = \frac{\log_2(N_L^0/N_A^0)}{\nu_A - \nu_L} \quad (7)$$

in the following we use this time as a reference to synchronize the three experiments (see figure 6).

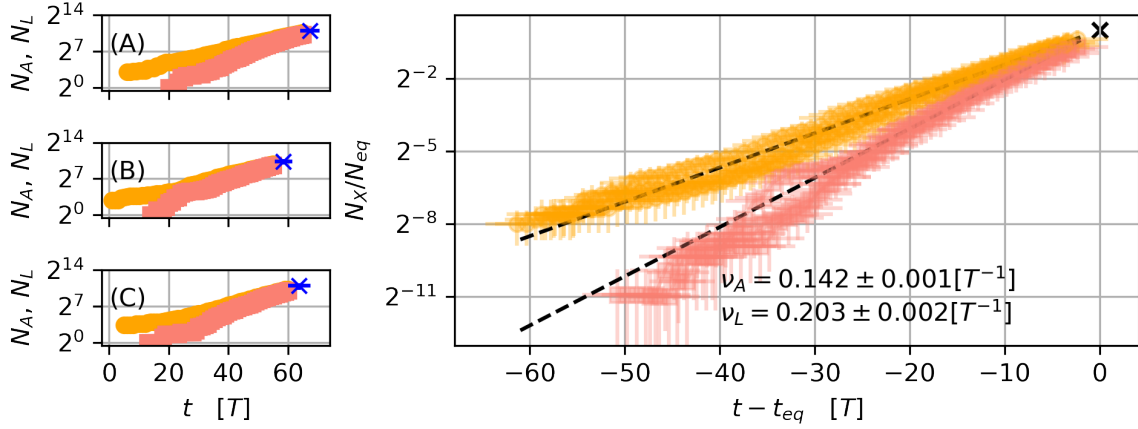


Figure 6: Left) counts of apical and lateral branch over time for the three experiments. Blue marker correspond to the point (t_{eq}, N_{eq}) for each experiment. Right) normalized count of apical and lateral branch over unified time for the three experiments. Dashed line correspond to mean exponential fits for apical (in orange) and lateral (in red).

Spatial distinction: Another metric interesting to look at is the respective position of such branching points. For this we consider the distributions of the ratio of the euclidean distance to the spore over the maximal radius of the thallus at the moment of branching for the two kinds of branching (see figure 7). In both apical and lateral case, this ratio appears to stabilize around a constant value over time although the maximum radius grows linearly with time. The difference in the value of this constant, $r_A = 0.65 \pm 0.03$ in the apical case and $r_L = 0.42 \pm 0.02$ in the lateral case, reflects a difference in the spatial occupation of these branches. Lateral branches are mainly found inside the thallus, while apical branches are found in the outer ring. Cumulative density estimate in figure 7 show that half the apical branches appear above $r \approx 0.66$ while almost all lateral branches appear below this value.

Dynamical distinction: Another distinction between apical and lateral branches is their elongation rate. In Figure 8, we have plotted the mean elongation \dot{L}_i for branches emerging from an apical branching point or a lateral one according to the time since the branch start growing (noted t_0 in the figure). We considered only branches growing over at least 12 frames, that corresponds to approximatively $860 \mu m$ long branch for apical ones and $625 \mu m$ for lateral ones. From respectively experiments *A*, *B* and *C* we extracted 96, 82 and 98 apical branches and 50, 51 and 53 lateral branches. We observe that in both cases the mean elongation start by an acceleration phase at an initial value $\dot{L}_i^0 \neq 0$ before reaching a steady-state at rate \dot{L}_i^f . We fitted the result according to the following empirical law:

$$\dot{L}_i(t) = (\dot{L}_i^f - \dot{L}_i^0) (1 - e^{-\gamma t}) + \dot{L}_i^0 \quad (8)$$

For apical branches we find $\dot{L}_i^0 = 2.5 \pm 0.2 \mu m/min$, $\dot{L}_i^f = 4.04 \pm 0.03 \mu m/min$ and $\gamma = 2.6 \pm 0.4 h^{-1}$ while for lateral branches we find $\dot{L}_i^0 = 0.78 \pm 0.07 \mu m/min$, $\dot{L}_i^f = 2.9 \pm 0.2 \mu m/min$ and $\gamma = 0.5 \pm 0.1 h^{-1}$.

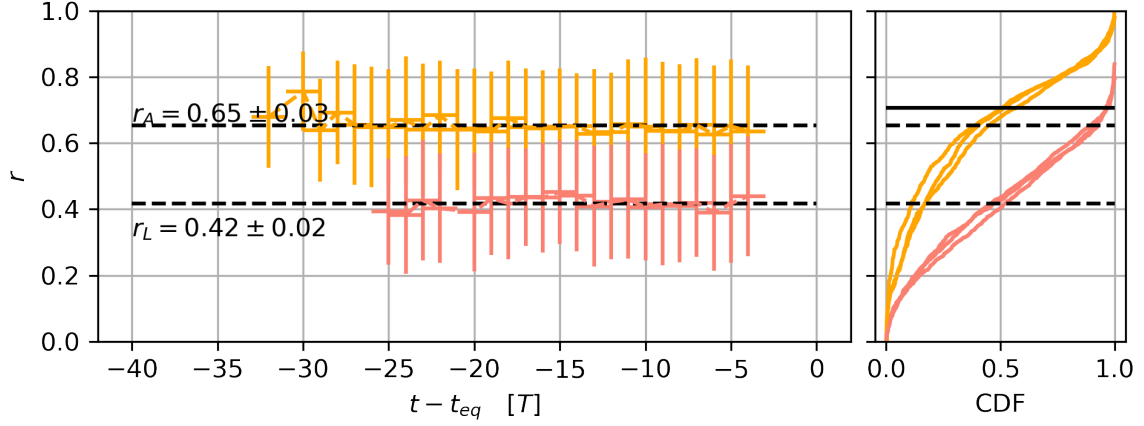


Figure 7: Left) Ratio of the euclidean distance to the spore over the maximal radius at the moment of branching for the apicals in orange and the laterals in red (mean \pm standard deviation) as a function of time. Right) Cumulative density estimate of this distributions. Dashed line corresponds to r_A mean value for apical branchings and r_L mean value for lateral branching. Solid black line correspond to the theoretical division where the outer ring has the same area as the inner disk.

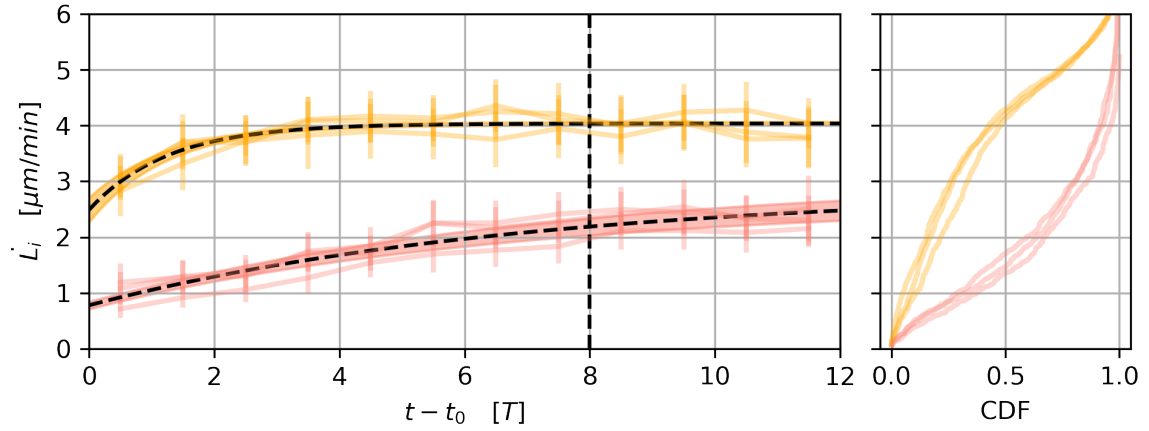


Figure 8: Left) Mean elongation \dot{L}_i as a function of time since the branch start $t - t_0$ for both apical (in orange) and lateral (in red). Dashed line correspond to the fit according to Equation 8. Right) Cumulative density estimate of elongations in the stationary domain ($t - t_0 \geq 8T$).

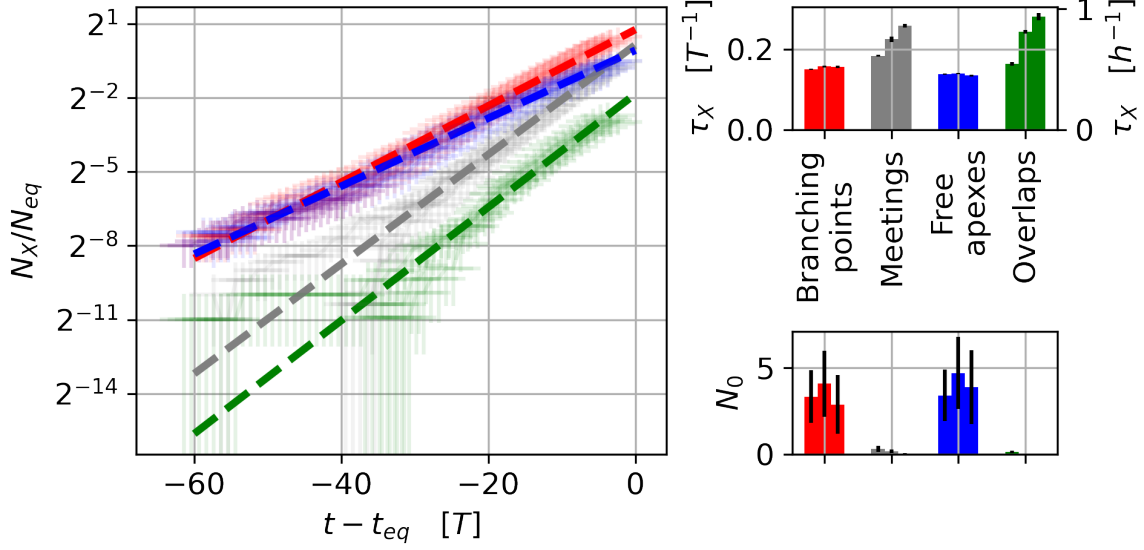


Figure 9: Counts of branching points (in red), free apices (in blue), encounters (in grey) and overlaps (in green) with respect to time normalized for each experiment (A), (B) and (C). Dashed lines correspond to mean fits for each counts of the form $N_X = N_0^X 2^{\tau_X t}$.

Count of the number of free apices, branching points, encounters and overlaps.

Dealing with a network cleaned of overlaps, with branches rebuilt in their entirety, we are now able to distinguish the different biological origins of degree-3 vertices. Direct counting of the number of biological objects in the network, branching point (lateral and apical), free apices and encounters are shown in figure 9. Encounters combine anastomosis and cessation of apex growth in the immediate vicinity of a hypha. To complete the description with non biological structures, the number of overlaps was added into the figure. It was reported in Dikec et al. [2020] an exponential growth over time of the total length of the network. In this work, we observe the same exponential behavior for the numeration of branching points, free apices, encounters and overlaps. We adjust these exponential growths in figure 9 according to the same expression as for the growth in number of apical and lateral branches described in equation 6 with X corresponding this time to branching points, free apices, encounters or overlaps. As expected, at the beginning of the growth, with a very simple network, only branching points and free apices are observed. With the increase in density, encounters and overlaps become more frequent. At the end of the experiment, about half of the branches no longer end in free apices, but in an encounter. Interestingly, overlaps and encounters growth rates are approximately similar, which suggests that the proportion of encounters that become overlaps does not depend on the stage of growth. This proportion (Number of overlaps divided by the sum of the number of overlaps and encounters) is calculated to be in average of $19 \pm 1\%$. We also note that the variability between experiments is greater than the variability between the different objects studied here (branches, free apices, encounters and overlaps).

Discussion

In this work, we propose to exploit images of the growth of the filamentous fungus thallus *P. anserina*, model of a growing and branching network. These images were obtained using a simple microscopic device, *i.e.* exploiting the possibilities offered by recent developments in image capture systems and the automation of spatial and temporal monitoring. Despite its advantages, fluorescence lighting has not been chosen. Our experimental system has the advantage of being sufficiently efficient in white light. This is an advantage insofar as, whenever possible, the use of white light illumination is preferable to fluorescence illumination, as it alleviates the experimental constraints linked to the fluorescent illumination device, the constraints linked to reconstruction (for instance alignment can be made tricky), and the effects of tissue ageing. Growing on a cellophane sheet enables two-dimensional guidance of the thallus, the simplicity of which allows high sampling frequency and easy reconstruction compared with three-dimensional techniques. The result is a collection of independent images that can be represented by a single graph, made up of interconnected nodes of degree-3 or less. Individual labeling of each object in the network is made problematic by the lack of articulation between images. In particular, the overlaps introduce an over-numeration of nodes of degree-3. Thanks to the tracking of apex trajectories through individual branch identification, we can identify overlaps as a combination of a branch ending in an encounter and a new branch synchronized in time and space along the same carrier branch. Comparison with a simulation has enabled us to estimate the good efficiency of our method in the range of parameter values encountered within experiments through different metrics such as the F-score and the Matthew Correlation Coefficient. Thanks to this reconstruction, we can identify the different branches of the network, allowing us to track any apex while retaining global information on network connectivity. To automatically determine the nature of this branches (apical or lateral), we propose a latency time criterion between the first passage of a hypha and the moment of branching. Below the threshold value Δt_{AL} , whose numerical value is obtained by adjusting latency times at the scale of the complete thallus, the branching is considered apical (and inversely lateral). At the start of the exponential growth phase, the network is composed solely of branches from an apical branch. However, as the mechanics are different in the two mechanisms (proportional to the number of apexes for apical branches and proportional to the total length of the network for lateral branches), the effective growth rate of lateral branches is higher than that of apical branches. This distinction removes the ambiguity surrounding the initial latent phase due to germination. This phase of random duration precedes the network's exponential growth phase. This makes it difficult to compare one experiment with another. We then define the instant t_{eq} when the two sub-populations (apical and lateral branches) are in the same number, *i.e.* $N_A(t_{eq}) = N_L(t_{eq})$. The latter can be used as a reference to compare growth times between different experiments. As reported in Ledoux et al. [2023], the density of the network depends directly on the branching activity of the apical and lateral types. The former follows an exponentially decreasing law from the apex, while the latter shows a continuous branching rate per unit length. The time lag observed between the two processes spontaneously generates a density minimum. We show here that the time lag is not the only factor involved, but is also coupled with a spatial difference in branch organization and a difference in branch growth dynamics. The thallus is an inhomogeneous object. The biological nature of the branches depends on their location relative to the origin (the spore) of the site observed, and the time between it and the passage of the growth front. The biological nature corresponds to lateral and apical branches. These two sub-populations grow in the same network, but with different branching mechanisms and elongation speeds. These behavior discrepancies are probably linked to various biological processes at cellular

level, still largely unknown, and governing both types of branching. Then, while apical branching usually involves a significant disturbance in the growth rate and morphology of the parental hyphal tip, with a temporary disappearance of the Spitzenkörper, lateral branching occurs without any detectable alterations in the growth or Spitzenkörper behaviour of the parental hypha (Riquelme et al. [2011]). Branches from apical branches are faster, earlier and located in the outer crown of the thallus. These characteristics, in addition to the asymmetrical branching angles (Ledoux et al. [2022]), make them ideal for exploration. Lateral branches are slower, later and tend to be located in the center of the thallus. These features, in addition to the typical 90-degree branching angles also reported in Ledoux et al. [2022], make them densification hyphae. It should be noted here that these results are in line with the functional description of the fungal thallus, reported several years ago. Then, Lew [2005] described the fungal network as consisting of apical cells (or leading hyphae) which are the first cells to invade new territory and are generally engaged in nutrient acquisition and sensing of the local environment, whereas behind the colony edge, sub-apical cells generate new hyphae by lateral branching. An earlier description of such fungal network states that hyphal tips at the biomass edge are those associated with exploration while hyphal tips behind the biomass front are most associated with resource exploitation (Boswell et al. [2002]). It is important to note that the distinction proposed in this work is based on a statistical approach. In the absence of a clear distinction between apical and lateral differences, the proposed studies were based on spatial location, with apical branches assumed to be favorably furthest from the spore. We justify this choice by noting the predominance of apical branches in the outer ring. We can be more precise and defined the outer ring according to the distance between the spore and the furthest apex. Beyond $r = \sqrt{2}/2$ there are statistically no more lateral branches, which corresponds to a division of the thallus into two zones, the outer ring and inner disk, of equal areas. Conversely, the type of branches present in the densest regions is statistically composed of lateral branches. To our knowledge, their specific study has never been undertaken. The reconstruction is based on the characteristics of the fungal thallus studied. Some of these can be lifted, enabling this work to be generalized to any growing network in two dimensions, biological or not, e.g. on cities or fractures. The origin of the network is assumed to be unique. This is necessary in the reconstruction of complex branches, whose causality cannot be deduced from observation, especially with very short segments. The multiple-source assumption is not allowed in the case presented here. However, this configuration can be found with growth ignition based on multiple ascospores or from fragmented mycelia. In this case, one way to overcome this difficulty could be to recognize them individually before processing. The filaments making up the network are considered identical, *i.e.* their diameter is not taken into account. This information could be easily retrieved, enabling the study of networks that reorganize themselves such as the one described in the slime moulds *Physarum polycephalum* (Reid [2023]) and adapt the flows passing through them by modifying their characteristics. Another characteristic of the blob is not taken into account in this work. A network can evolve by abandoning low-use connections, which can lead to necrosis. This work is based on a reference image containing the entire network. Insofar as the growth of *P. anserina* is not accompanied by retraction, a late image is compatible with this work. A reorganization of the network generated by an abandonment of connections, could be taken into account if the network were found to evolve between different well-defined states of maximum complexity. An extraction of the images corresponding to these states would enable the intermediate states to be reconstructed. Similarly, the network is expected to be fixed in the laboratory reference frame. If a node or connection were to slip, it could not be recovered.

Conclusion

Overall, the reconstruction of the dynamics of this network allows us to follow each apex over time (despite overlaps) and to identify each hypha individually, with the possibility of automatically categorizing the nature of the branching (apical or lateral) at its origin. This labelling makes it possible to automate several measurements that can then be applied rapidly to the entire network, such as measuring branching angles or elongation rates. The differences in dynamics and temporality according to the type of hyphal branching also highlight the different roles of hyphae between exploration and exploitation of the environment.

Author Contributions

F.C.L. and E.H. initiated the research. T.C. wrote the data extraction programmes and analyzed the data. All authors discussed the results and wrote the article.

Acknowledgments

The authors would like to thank Clara Ledoux for conducting the experiments, Frederic Filaine for the experimental set-up, Christophe Lalanne for his advice on statistical analyses, Aurélien Renault for the technical assistance. and the NEMATIC group for fruitful discussions. Thibault Chassereau is supported by a PhD scholarship from ANR-21-CE40010-01.

Declaration of interests

The authors declare no competing interests.

References

- Ryan A. Rossi and Nesreen K. Ahmed. The network data repository with interactive graph analytics and visualization. In *AAAI*, 2015. URL <https://networkrepository.com>.
- Jure Leskovec and Andrej Krevl. SNAP Datasets: Stanford large network dataset collection. <http://snap.stanford.edu/data>, June 2014.
- C. Lagesse, P. Bordin, and S. Douady. A spatial multi-scale object to analyze road networks. *Network Sci.*, 3(1):156–181, March 2015. ISSN 2050-1242. doi: 10.1017/nws.2015.4.
- S. Bohn, L. Pauchard, and Y. Couder. Hierarchical crack pattern as formed by successive domain divisions. *Phys. Rev. E*, 71(4):046214, April 2005. ISSN 2470-0053. doi: 10.1103/PhysRevE.71.046214.
- Paul Valcke. *Form, formation, deformation of Gorgonia ventalina : shape properties of spatial growing reticulated 2D trees in their mechanical environment*. PhD thesis, Université Paris Cité, Paris, France, November 2020. URL <https://theses.hal.science/tel-04210866>.

- Yoan Coudert, Steven Harris, and Bénédicte Charrier. Design Principles of Branching Morphogenesis in Filamentous Organisms. *Current Biology*, 29(21):R1149–R1162, November 2019. ISSN 0960-9822. doi: 10.1016/j.cub.2019.09.021. URL <https://www.sciencedirect.com/science/article/pii/S0960982219311819>.
- Ruth E Falconer, James L Bown, Nia A White, and John W Crawford. Biomass recycling and the origin of phenotype in fungal mycelia. *Proceedings of the Royal Society B: Biological Sciences*, 272(1573):1727–1734, August 2005. ISSN 0962-8452, 1471-2954. doi: 10.1098/rspb.2005.3150. URL <https://royalsocietypublishing.org/doi/10.1098/rspb.2005.3150>.
- Clara Ledoux, Cécilia Bobée, Éva Cabet, Pascal David, Frédéric Filaine, Sabrina Hachimi, Christophe Lalanne, Gwenaél Ruprich-Robert, Éric Herbert, and Florence Chapeland-Leclerc. Characterization of spatio-temporal dynamics of the constrained network of the filamentous fungus *Podospira anserina* using a geomatics-based approach. *PLOS ONE*, 19(2):e0297816, February 2024. ISSN 1932-6203. doi: 10.1371/journal.pone.0297816. URL <https://journals.plos.org/plosone/article?id=10.1371/journal.pone.0297816>. Publisher: Public Library of Science.
- Guillermo Vidal-Diez de Ulzurrun, Tsung-Yu Huang, Ching-Wen Chang, Hung-Che Lin, and Yen-Ping Hsueh. Fungal feature tracker (FFT): A tool for quantitatively characterizing the morphology and growth of filamentous fungi. *PLOS Computational Biology*, 15(10):e1007428, October 2019. ISSN 1553-7358. doi: 10.1371/journal.pcbi.1007428. URL <https://journals.plos.org/ploscompbiol/article?id=10.1371/journal.pcbi.1007428>.
- Liselotte De Ligne, Guillermo Vidal-Diez de Ulzurrun, Jan M. Baetens, Jan Van den Bulcke, Joris Van Acker, and Bernard De Baets. Analysis of spatio-temporal fungal growth dynamics under different environmental conditions. *IMA Fungus*, 10(1):7, June 2019. ISSN 2210-6359. doi: 10.1186/s43008-019-0009-3. URL <https://doi.org/10.1186/s43008-019-0009-3>.
- Graeme P. Boswell, Helen Jacobs, Fordyce A. Davidson, Geoffrey M. Gadd, and Karl Ritz. Functional consequences of nutrient translocation in mycelial fungi. *Journal of Theoretical Biology*, 217(4):459–477, August 2002. ISSN 0022-5193.
- Daniel P Bebbber, Juliet Hynes, Peter R Darrah, Lynne Boddy, and Mark D Fricker. Biological solutions to transport network design. *Proceedings of the Royal Society B: Biological Sciences*, 274(1623):2307–2315, July 2007. doi: 10.1098/rspb.2007.0459. URL <https://royalsocietypublishing.org/doi/10.1098/rspb.2007.0459>. Publisher: Royal Society.
- A. P. J. Trinci. The hyphal growth unit of wild type and spreading colonial mutants of *Neurospora crassa*. *Archiv für Mikrobiologie*, 91(2):127–136, June 1973a. ISSN 1432-072X. doi: 10.1007/BF00424756. URL <https://doi.org/10.1007/BF00424756>.
- A.P.J. Trinci. A Study of the Kinetics of Hyphal Extension and Branch Initiation of Fungal Mycelia. *Journal of General Microbiology*, 81:225–236, 1973b.
- M.d. Fricker, J.a. Lee, D.p. Bebbber, M. Tlalka, J. Hynes, P.r. Darrah, S.c. Watkinson, and L. Boddy. Imaging complex nutrient dynamics in mycelial networks. *Journal of Microscopy*, 231(2):317–331, 2008. ISSN 1365-2818. doi: 10.1111/j.1365-2818.2008.02043.x. URL <https://onlinelibrary.wiley.com/doi/abs/10.1111/j.1365-2818.2008.02043.x>. eprint: <https://onlinelibrary.wiley.com/doi/pdf/10.1111/j.1365-2818.2008.02043.x>.

- Cristina G. Reynaga-Peña, Gerhard Gierz, and Salomon Bartnicki-Garcia. Analysis of the role of the Spitzenkörper in fungal morphogenesis by computer simulation of apical branching in *Aspergillus niger*. *Proceedings of the National Academy of Sciences*, 94(17):9096–9101, August 1997. doi: 10.1073/pnas.94.17.9096. URL <https://www.pnas.org/doi/full/10.1073/pnas.94.17.9096>. Publisher: Proceedings of the National Academy of Sciences.
- G. W. Gooday. An Autoradiographic Study of Hyphal Growth of Some Fungi. *Journal of General Microbiology*, 67(1):125–133, 1971.
- David J Barry, Cecilia Chan, and Gwilym A Williams. Morphological quantification of filamentous fungal development using membrane immobilization and automatic image analysis. *Journal of Industrial Microbiology and Biotechnology*, 36(6):787, June 2009. ISSN 1367-5435. doi: 10.1007/s10295-009-0552-9. URL <https://doi.org/10.1007/s10295-009-0552-9>.
- Gamaliel Sánchez-Orellana, Sergio Casas-Flores, and Braulio Gutiérrez-Medina. Automated, continuous video microscopy tracking of hyphal growth. *Fungal genetics and biology: FG & B*, 123: 25–32, November 2018. ISSN 1096-0937. doi: 10.1016/j.fgb.2018.11.006.
- Stefanie S. Schmieder, Claire E. Stanley, Andrzej Rzepiela, Dirk van Swaay, Jerica Sabotič, Simon F. Nørrelykke, Andrew J. deMello, Markus Aebi, and Markus Künzler. Bidirectional Propagation of Signals and Nutrients in Fungal Networks via Specialized Hyphae. *Current Biology*, 29(2): 217–228.e4, January 2019. ISSN 0960-9822. doi: 10.1016/j.cub.2018.11.058. URL <https://www.sciencedirect.com/science/article/pii/S0960982218315574>.
- G. Vidal-Diez de Ulzurrun, J. M. Baetens, J. Van den Bulcke, C. Lopez-Molina, I. De Windt, and B. De Baets. Automated image-based analysis of spatio-temporal fungal dynamics. *Fungal Genetics and Biology*, 84:12–25, November 2015. ISSN 1087-1845. doi: 10.1016/j.fgb.2015.09.004. URL <http://www.sciencedirect.com/science/article/pii/S1087184515300281>.
- Mark D. Fricker, Luke L. M. Heaton, Nick S. Jones, and Lynne Boddy. The Mycelium as a Network. *Microbiology Spectrum*, 5(3):10.1128/microbiolspec.funk-0033-2017, May 2017. doi: 10.1128/microbiolspec.funk-0033-2017. URL <https://journals.asm.org/doi/10.1128/microbiolspec.funk-0033-2017>. Publisher: American Society for Microbiology.
- J. Dikec, A. Olivier, C. Bobée, Y. D’Angelo, R. Catellier, P. David, F. Filaine, S. Herbert, Ch Lalanne, H. Lalucque, L. Monasse, M. Rieu, G. Ruprich-Robert, A. Véber, F. Chapeland-Leclerc, and E. Herbert. Hyphal network whole field imaging allows for accurate estimation of anastomosis rates and branching dynamics of the filamentous fungus *Podospira anserina*. *Scientific Reports*, 10(1):1–16, February 2020. ISSN 2045-2322. doi: 10.1038/s41598-020-57808-y. URL <https://www.nature.com/articles/s41598-020-57808-y>.
- Huan Du, Pin Lv, Mehdi Ayouz, Arnaud Besserer, and Patrick Perré. Morphological Characterization and Quantification of the Mycelial Growth of the Brown-Rot Fungus *Postia placenta* for Modeling Purposes. *PLOS ONE*, 11(9):e0162469, September 2016. ISSN 1932-6203. doi: 10.1371/journal.pone.0162469. URL <https://journals.plos.org/plosone/article?id=10.1371/journal.pone.0162469>. Publisher: Public Library of Science.
- Ann-Shyn Chiang, Chih-Yung Lin, Chao-Chun Chuang, Hsiu-Ming Chang, Chang-Huain Hsieh, Chang-Wei Yeh, Chi-Tin Shih, Jian-Jheng Wu, Guo-Tzau Wang, Yung-Chang Chen, Cheng-

- Chi Wu, Guan-Yu Chen, Yu-Tai Ching, Ping-Chang Lee, Chih-Yang Lin, Hui-Hao Lin, Chia-Chou Wu, Hao-Wei Hsu, Yun-Ann Huang, Jing-Yi Chen, Hsin-Jung Chiang, Chun-Fang Lu, Ru-Fen Ni, Chao-Yuan Yeh, and Jenn-Kang Hwang. Three-Dimensional Reconstruction of Brain-wide Wiring Networks in *Drosophila* at Single-Cell Resolution. *Current Biology*, 21(1):1–11, January 2011. ISSN 0960-9822. doi: 10.1016/j.cub.2010.11.056. URL [https://www.cell.com/current-biology/abstract/S0960-9822\(10\)01522-8](https://www.cell.com/current-biology/abstract/S0960-9822(10)01522-8). Publisher: Elsevier.
- Stefan Schmideder, Lars Barthel, Henri Müller, Vera Meyer, and Heiko Briesen. From three-dimensional morphology to effective diffusivity in filamentous fungal pellets. *Biotechnology and Bioengineering*, 116(12):3360–3371, 2019. ISSN 1097-0290. doi: 10.1002/bit.27166. URL <https://onlinelibrary.wiley.com/doi/abs/10.1002/bit.27166>. eprint: <https://onlinelibrary.wiley.com/doi/pdf/10.1002/bit.27166>.
- Philippe Silar. *Podospora anserina*. February 2020. URL <https://hal.science/hal-02475488>.
- Amir Sanati Nezhad and Anja Geitmann. The cellular mechanics of an invasive lifestyle. *Journal of Experimental Botany*, 64(15):4709–4728, November 2013. ISSN 1460-2431. doi: 10.1093/jxb/ert254.
- Clara Ledoux, Florence Chapeland-Leclerc, Gwenaël Ruprich-Robert, Cécilia Bobée, Christophe Lalanne, Éric Herbert, and Pascal David. Prediction and experimental evidence of the optimisation of the angular branching process in the thallus growth of *Podospora anserina*. *Scientific Reports*, 12(1):12351, July 2022. ISSN 2045-2322. doi: 10.1038/s41598-022-16245-9. URL <https://www.nature.com/articles/s41598-022-16245-9>. Number: 1 Publisher: Nature Publishing Group.
- Clara Ledoux, Florence Chapeland-Leclerc, Gwenaël Ruprich-Robert, Cécilia Bobée, Christophe Lalanne, Éric Herbert, and Pascal David. Prediction and experimental evidence of different growth phases of the *Podospora anserina* hyphal network. *Scientific Reports*, 13(1):8501, May 2023. ISSN 2045-2322. doi: 10.1038/s41598-023-35327-w. URL <https://www.nature.com/articles/s41598-023-35327-w>. Number: 1 Publisher: Nature Publishing Group.
- Davide Chicco and Giuseppe Jurman. The advantages of the Matthews correlation coefficient (MCC) over F1 score and accuracy in binary classification evaluation. *BMC Genomics*, 21(1):1–13, December 2020. ISSN 1471-2164. doi: 10.1186/s12864-019-6413-7.
- Meritxell Riquelme, Oded Yarden, Salomon Bartnicki-Garcia, Barry Bowman, Ernestina Castro-Longoria, Stephen J. Free, Andre Fleißner, Michael Freitag, Roger R. Lew, Rosa Mouriño-Pérez, Michael Plamann, Carolyn Rasmussen, Corinna Richthammer, Robert W. Roberson, Eddy Sanchez-Leon, Stephan Seiler, and Michael K. Watters. Architecture and development of the *Neurospora crassa* hypha – a model cell for polarized growth. *Fungal Biology*, 115(6):446–474, June 2011. ISSN 18786146. doi: 10.1016/j.funbio.2011.02.008. URL <https://linkinghub.elsevier.com/retrieve/pii/S1878614611000298>.
- Roger R. Lew. Mass flow and pressure-driven hyphal extension in *Neurospora crassa*. *Microbiology*, 151(8):2685–2692, August 2005. ISSN 1350-0872, 1465-2080. doi: 10.1099/mic.0.27947-0. URL <https://www.microbiologyresearch.org/content/journal/micro/10.1099/mic.0.27947-0>.

Chris R. Reid. Thoughts from the forest floor: a review of cognition in the slime mould *Physarum polycephalum*. *Animal Cognition*, 26(6):1783–1797, November 2023. ISSN 1435-9448, 1435-9456. doi: 10.1007/s10071-023-01782-1. URL <https://link.springer.com/10.1007/s10071-023-01782-1>.

Distribution of latency before branching

We aim to derive an expression for the observable $\mathcal{B}_{t_i}^{t_f}(\Delta t)$, the number of branchings occurring during the period $t \in [i T; f T[$ and appearing after a latency time $\Delta t \in [j T; (j+1) T[$, where $1/T$ is the frame rate and i, f, j are integers. The time origin is defined locally for each network node by the growth of the hypha at that point. Technically, the passage of an apex is detected. $\mathcal{B}_{t_i}^{t_f}(\Delta t)$ can be expressed as the sum of the corresponding apical branching $\mathcal{A}_{t_i}^{t_f}(\Delta t)$ and lateral branching $\mathcal{L}_{t_i}^{t_f}(\Delta t)$:

$$\mathcal{B}_{t_i}^{t_f}(\Delta t) = \mathcal{A}_{t_i}^{t_f}(\Delta t) + \mathcal{L}_{t_i}^{t_f}(\Delta t) \quad (9)$$

Apical part In this section we will build $\mathcal{A}_{t_i}^{t_f}(\Delta t)$ the apical contribution of $\mathcal{B}_{t_i}^{t_f}(\Delta t)$. Introducing $A(t_i, t_f)$ as the total number of apical branchings appearing between t_i and t_f and $\phi_A(\Delta t)$ as the probability for an apical branching to occur after Δt , we then write:

$$\mathcal{A}_{t_i}^{t_f}(\Delta t) = A(t_i, t_f) \phi_A(\Delta t)$$

At each time step, the number of apical branches appearing in the network is proportional to the number of apexes present in the network, which corresponds to the number of branches N (from apical or lateral branching). With τ_A the proportionality coefficient, we write $A(t_i, t_f)$ as

$$A(t_i, t_f) = \tau_A \int_{t_i}^{t_f} N(t) dt = \tau_A \frac{N(t_f) - N(t_i)}{\nu \log 2}$$

with $N(t) = N_0 2^{\nu t}$. Following Ledoux et al. [2023] we expect apical branching on a single hypha to be exponentially distributed from the tip, with a parameter ω_A . Following we can derive $\phi_A(\Delta t)$ as

$$\phi_A(\Delta t) = e^{-\omega_A \Delta t} \frac{1 - e^{-\omega_A T}}{1 - e^{-\omega_A (t_f - t_i + T)}}$$

which is normalized over all latencies, *i.e.* such that $\sum_{\Delta t=0}^{t_f - t_i} \phi_A(\Delta t) = 1$.

Lateral part We will now focus on $\mathcal{L}_{t_i}^{t_f}(\Delta t)$. Along a single hypha, we expect lateral branching to be distributed uniformly along the hypha except in the dominance apical region near the tip (see Figure 10). We modeled this property by modulating the lateral branching rate τ_L according to a sigmoid of parameter m and s depending on the latency Δt . Unlike the apical branchings, we assume that the number of lateral branchings appearing at time t is proportional to the total length

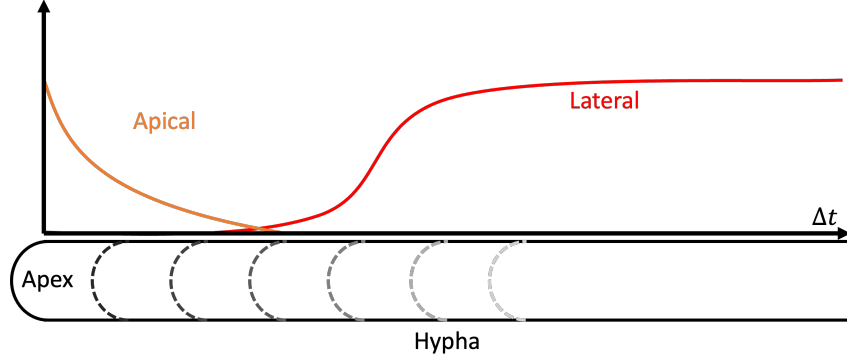


Figure 10: Diagram illustrating the distribution of apical (in orange) and latera (in red) branches along a single hypha.

of the network $L(t) = L_0 2^{\lambda t}$. By noticing $\frac{\tau_L}{1+e^{-(\Delta t-m)/s}}$ does not depend on t , we get:

$$\begin{aligned}\mathcal{L}_{t_i}^{t_f}(\Delta t) &= \int_{t_i+\Delta t}^{t_f} dt \frac{\tau_L}{1+e^{-(\Delta t-m)/s}} (L(t-\Delta t) - L(t-\Delta t-T)) \\ &= \frac{\tau_L}{1+e^{-(\Delta t-m)/s}} (1-2^{-\lambda T}) \frac{L(t_f-\Delta t) - L(t_i)}{\lambda \log 2}\end{aligned}$$

Finally equation 9 can be rewritten to obtain equation (4) of the main text:

$$\begin{aligned}\mathcal{B}_{t_i}^{t_f}(\Delta t) &= \tau_A \frac{N(t_f) - N(t_i)}{\nu \log 2} e^{-\omega_A \Delta t} \frac{1 - e^{-\omega_A T}}{1 - e^{-\omega_A(t_f-t_i+T)}} \\ &\quad + \frac{\tau_L}{1+e^{-(\Delta t-m)/s}} (1-2^{-\lambda T}) \frac{L(t_f-\Delta t) - L(t_i)}{\lambda \log 2}\end{aligned}\tag{10}$$

ν , N_0 , λ and L_0 can be determined from the fits of respectively N and L as a function of time t . Following, fit $\mathcal{B}_{t_i}^{t_f}(\Delta t)$ (see figure (6) of the main text) allowed us to extract ω_A , τ_A , τ_L , m and s . The corresponding experimental values are shown in table 1.